

# An Efficient and Reconfigurable Synchronous Neuron Model

H. Soleimani, E. M. Drakakis

## Abstract

This paper presents a reconfigurable and efficient two-dimensional (2-D) neuron model capable of extending to higher dimensions. The model is applied to the Izhikevich and FitzHugh–Nagumo neuron models as 2-D case studies and to the Hindmarsh–Rose model as a 3-D case study. Hardware synthesis and physical implementations show that the resulting circuits can reproduce neural dynamics with acceptable precision and considerably low hardware overhead compared to previously published piecewise linear models.

## 1 Introduction

paper proposes a reconfigurable and efficient "synchronous" neuron model capable of mimicking various biological neurons' dynamics with good precision and low hardware cost. Unlike the "asynchronous" cellular neuron models introduced in [1–2], the synchronous property of the proposed model would make the approach appropriate for large-scale pipelined implementations since the effective operating frequency is not limited by the asynchronous time delay between each step. Another advantage of the proposed model compared to [1–2] is the output coding of the system, in which the *membrane* and *recovery* registers change the output states through a relatively complex circuit with a one-hot bit coding. This coding scheme limits the state variables to be changed in a few locations and the higher the needed accuracy, the more complexity is applied to the hardware. In contrast, in the proposed approach, the output registers do not directly carry the address of the next velocity value that should be fetched from memory in the next clock. This implies that the output register can be set in any precision and not limited by the number of memory pixels. In other words, the proposed model is internally cellular and externally noncellular, while the model introduced in [1–2] is fully cellular which limits the output resolution leading to lower precision.

The rest of the paper is organized as follows: in Section II, the concept of synchronous cellular neuron model is presented. Section III investigates various hardware responses of the proposed model for 2-D case studies along with a higher dimension neuron model. The truncation error of the proposed system is discussed in Section IV. The synthesis results accompanied by an extensive comparison between the proposed and previous piecewise neuron models are presented in Section VI. Section VII concludes the paper.

## 2 Synchronous Cellular Neuron Model

In this model, according to [1], first we convert the phase plane of the biological neuron models into a 2-D cellular space where  $(x, y) \in Z^2$  represents the location of state point in the phase plane, and  $(\frac{dx}{dt}, \frac{dy}{dt})$  determines the velocity and direction of the motion. The x-nullcline is the set of points where  $\frac{dx}{dt} = 0$ . Similarly, y-nullcline is the set of points where  $\frac{dy}{dt} = 0$ . Clearly the points of intersection between x-nullcline and y-nullcline are the equilibrium points. Most 2-D neuron models can be rewritten in a general form as follows:

$$\begin{cases} \frac{dx}{dt} = F(x) + \alpha y + IN \\ \frac{dy}{dt} = G(x) + \beta y \end{cases} \quad (1)$$

In the cellular space,  $X[n] = i$  where  $i \in \mathbf{N} \equiv 0, 1, \dots, N - 1$  and  $Y[n] = j$  where  $j \in \mathbf{M} \equiv 0, 1, \dots, M - 1$  are discrete variables corresponding to  $x$  and  $y$  in the continuous space. The location of each state point in the  $\mathbf{N} \times \mathbf{M}$  cellular space can be defined as:

$$\begin{cases} X[n] = \lfloor \frac{x[n] - x_{min}}{\Delta x} \rfloor & ; & x[n] \in [x_{min}, x_{max}) \\ Y[n] = \lfloor \frac{y[n] - y_{min}}{\Delta y} \rfloor & ; & y[n] \in [y_{min}, y_{max}) \end{cases} \quad (2)$$

where  $\Delta x = \frac{x_{max} - x_{min}}{N}$  and  $\Delta y = \frac{y_{max} - y_{min}}{M}$ . Since most 2-D neuron models can be expressed in the form of (1) and  $F(x)$ ,  $G(x)$  are functions of  $x$ , the  $Y[n]$  introduced in (2) is not involved in the stored velocity functions

and we have:

$$\begin{cases} X_{null}(X[n-1]) = F(x_{min} + X[n-1] \cdot \Delta x) \\ Y_{null}(X[n-1]) = G(x_{min} + X[n-1] \cdot \Delta x) \end{cases} \quad (3)$$

where  $X_{null}$  and  $Y_{null}$  are portions of time continuous nullclines and the next state of each dynamical variable is obtained by:

$$\begin{cases} x[n] - x[n-1] = \Delta t \cdot [X_{null}(X[n-1]) + \alpha y[n-1]] \\ + \Delta t \cdot IN \\ y[n] - y[n-1] = \Delta t \cdot [Y_{null}(X[n-1]) + \beta y[n-1]] \end{cases} \quad (4)$$

where  $[n]$  and  $[n-1]$  represent the current and previous states respectively. As can be seen, the proposed cellular model is independent of the neuron model's complexity since both  $X_{null}$  and  $Y_{null}$  are stored off-line. Moreover, the value of each state variable is synchronously changed, implying that the timing of both state variables is equal. Clearly, the address of the next cellular state is indirectly related to the output variables. This feature allows the output value to work in any precision leading to increased accuracy compared to the previous cellular models [1–2].

The direction of new motions on the cellular space can be formulated as:

$$\begin{cases} X[n] - X[n-1] = 0 \Rightarrow \text{"no change"} \\ X[n] - X[n-1] \geq 1 \Rightarrow \text{"upward motion"} \\ X[n] - X[n-1] \leq -1 \Rightarrow \text{"downward motion"} \end{cases} \quad (5)$$

It should be stressed that the resultant motion on the 2-D cellular phase planes is determined only by the motion in  $X$  direction and the number of motions on the cellular space unlike the one-hot bit coding in [1–2] can be more than one step in each clock cycle.

### 3 Hardware Architecture

In this section, according to the cellular mapping introduced in the previous section, we present two digital architectures describing a single and a network of neuron units.

#### 3.1 Single Digital Cellular Model

This circuit contains three major parts demonstrated in Fig. 1 (a):

##### 3.1.1 Storage Blocks

As concluded from the previous section, we calculate the  $X_{null}$  and  $Y_{null}$  arrays and store them in a set of registers. The stored vectors are programmed off-line, using (3) in accordance to predetermined model parameters. For a 2-D neuron model, these signed values are stored in two sets of registers with the size of  $N$  and  $M$  for both  $X$  and  $Y$  respectively. The size of each nullcline's component is 18 bits and the corresponding values are fetched for both state variables according to the address of  $X$ .

##### 3.1.2 Next State Provider

This block contains five adders, two multiplexers and two shifts to provide the next state of the dynamical variables. According to (4), the values fetched from the storage blocks ( $X_{null}$  or  $Y_{null}$ ) are added to a portion of  $y^-$ , the time-dependent input (if applicable) and then shifted as  $dt$ . The result is added to the previous state of the dynamical variable. The obtained value is filtered according to the reset condition. The absolute value of the output for each dimension represents the amount of state-variable increase or decrease in each step. Thus, higher values lead to increasing state variable. Clearly, the reason why we term the cellular model "synchronous" is that in each clock cycle the dynamical variables evolve equally in time.

##### 3.1.3 Addresser

The location of each state variable in the cellular phase plane is calculated in this block. In other words, this block is responsible for converting the non-cellular output variables to cellular addresses in order to fetch the next value from the storage blocks. Since the 2-D neuron models can be represented by (1), we need only one addresser block for both dimensions. This conversion can be easily implemented using (2) and by one subtract and one shift operation when the values  $x_{min}$ ,  $x_{max}$  and  $N$  are properly chosen (these values are presented for each neuron model in Table I).

### 3.2 Network of Digital Cellular Neuron

Since the critical path in the proposed cellular model is determined only by one subtractor embedded in the *Addresser Block* (see Fig.1(b)), the digital hardware can be easily shared for large-scale simulation of spiking neural networks. To this end, a network of pipelined neuron units is presented, capable of real-time operation. The number of real-time neuron units that can be accommodated in this structure depends on the operating frequency and time step (i.e. clock frequency $\times$ dt). As illustrated in Fig. 1(b),  $X_{buffers}$  and  $Y_{buffers}$  are added to the single cellular model to store the data of each neuron unit. These buffers are shifted in each clock pulse and the proper output is fed to the *Addresser Block* to provide the next cellular address and to the *Next State Provider* as the previous state of the dynamical system.

## 4 Hardware Time Domain Results

### 4.1 2-D Neuron Models

In this section, we map the proposed cellular approach on two well-known 2-D neuron models and then synthesize them on a high-performance Kintex-7 (XC7K325T) FPGA according to the architecture introduced in the previous section.

The first test case is the Izhikevich neuron model [3] capable of mimicking a wide range of firing patterns and their underlying bifurcation scenarios. The mathematical description of this model is denoted by:

$$\begin{cases} \dot{v} = 0.04v^2 + 5v + 140 - u + I \\ \dot{u} = a \cdot (b \cdot v - u) \end{cases} \quad (6)$$

$$\text{if } v > 30\text{mV} \text{ then } \begin{cases} v \leftarrow c \\ u \leftarrow u + d \end{cases} \quad (7)$$

where  $v$  represents the membrane potential of the neuron,  $u$  represents a membrane recovery variable and  $a, b, c, d$  are dimensionless parameters. According to the cellular mapping introduced in section II, the model can be rewritten in the general form of (1) and then can be conveniently mapped on the proposed architecture as follows:

$$\begin{cases} x = v, y = u \\ \alpha = 1, \beta = a \\ F(x) = 0.04x^2 + 5x + 140 \\ G(x) = b \cdot x \end{cases} \quad (8)$$

Fig. 2 illustrates the hardware results on a digital oscilloscope for various time domain waveforms produced by the synchronous cellular approach. As can be seen in the figure, there is remarkable compliance between the hardware results and the biological counterpart [3].

The second neuron model test case is the FHN (FitzHugh-Nagumo) model [4] which is a two-dimensional simplification of the Hodgkin-Huxley model. Its equations are given by:

$$\begin{cases} \dot{v} = v - \frac{v^3}{3} - u + I \\ \dot{u} = a \cdot (v + 0.7 - 0.8u) \end{cases} \quad (9)$$

where  $v$  is the membrane potential variable,  $u$  is the recovery variable,  $I$  is the input stimulus current, and  $a$  is a dimensionless parameter. The FHN model can be also re-expressed in the form of (1) and then easily mapped on the proposed platform:

$$\begin{cases} x = v, y = u \\ \alpha = 1, \beta = 0.8a \\ F(x) = x - \frac{v^3}{3} \\ G(x) = (x + 0.7)/0.8 \end{cases} \quad (10)$$

Fig. 3 (a-h) illustrates the hardware results on a digital oscilloscope for four significant phenomena of the FHN model reproduced by the cellular model. As can be seen in the figure, the hardware results obtained from the proposed structure are practically identical compared to the biological ones [4].

### 4.2 3-D Neuron Models

In order to show the applicability of the proposed cellular model in higher dimensions, in this section, we apply the approach on the Hindmarsh-Rose (HR) neuron model [5] as a 3-D case study. The dynamical behavior of the HR neuron model is given by:

$$\begin{cases} \dot{v} = u - v^3 + 3v^2 - k + I \\ \dot{u} = 1 - 5v^2 - u \\ \dot{k} = r(4(v + \frac{8}{5}) - k) \end{cases} \quad (11)$$

In this model,  $v$  is the membrane potential,  $u$  is the spiking variable,  $k$  is the bursting variable and  $I$  is the applied neuron current. The equations can be re-expressed as:

$$\begin{cases} x[n] - x[n-1] = \Delta t \cdot [F(x[n-1]) + \alpha y[n-1] + \gamma z[n-1]] \\ y[n] - y[n-1] = \Delta t \cdot [G(x[n-1]) + \beta y[n-1]] \\ z[n] - z[n-1] = \Delta t \cdot [H(x[n-1]) + \lambda z[n-1]] \end{cases} \quad (12)$$

where

$$\begin{cases} x = v, y = u, z = k, \\ \alpha = 1, \gamma = -1, \beta = -1, \lambda = -r \\ F(x) = x^3 - 3x^2 \\ G(x) = 1 - 5x^2 \\ H(x) = r(4(x + \frac{8}{5})) \end{cases} \quad (13)$$

Fig. 3 (i-l) shows the hardware results on a digital oscilloscope for two spiking and bursting modes produced by the synchronous cellular approach. As can be seen in the figure, the cellular model is able to reproduce high precision time domain waveforms, very close to the biological model [5].

Note that, due to a lack of space, bifurcation analyses are not presented here, however it has been confirmed at least for two important bifurcations (saddle node on/off invariant circle) that the proposed cellular model can reproduce similar mechanisms in a fair manner.

## 5 Truncation Error

As explained before, the approach detailed in this work converts the continuous nullclines into a cellular space with discrete cells locating any point with an address prepared by the dynamical system's outputs. This conversion allows our synchronous approach to track any trajectory in the phase plane when discretized by a sufficient number of pixels. However, depending on the cellular space dimension, a truncation error can be observed in the system after each clock cycle. In this section, we formulate this error for a 2-D dynamical system and discuss its sources and how to determine an optimum hardware architecture. First, let us assume that  $dt$  is small enough and its corresponding error is negligible. Now, if we fetch the cellular nullclines values from the storage blocks, the next state variables are:

$$\begin{cases} x[n]_{cellular} = \overbrace{x[n-1] + dt[F(x[n-1]) + \alpha y[n-1] + IN]}^{x_{continuous}} \pm \epsilon_1 \\ y[n]_{cellular} = \overbrace{y[n-1] + dt[G(x[n-1]) + \beta y[n-1]]}^{y_{continuous}} \pm \epsilon_2 \end{cases} \quad (14)$$

where  $\epsilon_1$  and  $\epsilon_2$  are the differences between the continuous nullclines values and the corresponding cellular values. Thus, the address of the next cellular values fetched from the storage registers for both dimensions is given by:

$$X[n] = \lfloor \frac{x[n]_{continuous} \pm \epsilon_1 - x_{min}}{\Delta x} \rfloor \quad (15)$$

This implies that the value of  $\epsilon_1$  and the floor function both contribute to the truncation error in the system since the  $X[n]$  must be an integer for both addresses. This truncation error takes the form of momentary and permanent lag/lead deviations in the time domain signals. However, the cellular trajectories can track well the continuous ones in the phase plane under certain conditions on the number of pixels (i.e. the error is reduced by increasing the number of pixels).

## 6 Error Analysis

As a consequence of the aforementioned truncation error, here we define a root mean square error (RMSE) to measure the time domain error of the proposed cellular system ( $V_c$ ) compared to the original biological model ( $V_o$ ). The error criterion is defined as follows:

$$\text{RMSE}(V_c, V_o) = \sqrt{\frac{\sum_{i=1}^n (V_c - V_o)^2}{n}} \quad (16)$$

where the normalized root mean square error (NRMSE) is described by:

$$\text{NRMSE} = \frac{\text{RMSE}}{V_{\text{max}} - V_{\text{min}}}. \quad (17)$$

The measured time domain error for 1000 points of some cases of neuron models with various resolutions is shown in Table II. The results show that by increasing the number of pixels, the error is decreased as predicted in the previous section.

## 7 Hardware Synthesis Results

The concept of employing digital piecewise linear models in neuromorphic engineering was first introduced in [6], and since then a number of valuable attempts were accomplished following the same general track [6–8]. The basic idea behind these works is how to modify the critical path in the digital designs while preserving the time domain and phase domain properties of the biological model. For a fair comparison between the proposed cellular model and previously published piecewise linear models, the design is first synthesized on a Xilinx Virtex-II Pro (XC2VP30) FPGA. Device utilization details for the synthesis of the cellular and other piecewise linear models are summarized in Table III, IV and V.

The results confirm that thanks to the efficient design of the cellular model (and as expected), a smaller area and a higher clock frequency are achieved compared to previously published piecewise linear neuron models. Since there are only 4-input LUTs (16-bits maximum) in the Xilinx Virtex-II Pro (XC2VP30) FPGA, each stored nullcline's component with 18 bits cannot be accommodated in one LUT, leading to a more complex routing process with lower operating frequency for the cellular model. Therefore, the cellular models are also synthesized on the Kintex-7 (XC7K325T) FPGA containing 6-input LUTs fabricated by more advanced technology. The synthesis results show a higher speed operating frequency and lower LUT usage as anticipated. The device utilization for this experiment is summarized in Table VI.

## 8 Conclusion

This paper presented a reconfigurable cellular model, independent of the neuron model's complexity (for those that can be written in the general form of (1)). Findings showed that the proposed model reproduces very well the targeted neurodynamics and applies no serious constraint on the critical path of the system. To verify the performance of the cellular model, two architectures were designed and realized on the Kintex-7 (XC7K325T) FPGA describing a single and a network of neuron units. Hardware synthesis results showed that the proposed cellular model has reached a lower area usage and higher speed in comparison with previously published piecewise neuron models. Moreover, as an extension of the approach, a 3-D neuron model was mapped onto the system with promising results in terms of accuracy and hardware cost.

## 9 Acknowledgement

This work is supported by funding from the Hans Rausing Scholarship.

## References

- [1] M. Bavandpour, H. Soleimani, B. Linares-Barranco, D. Abbott and L. O. Chua, "Generalized reconfigurable memristive dynamical system (MDS) for neuromorphic applications," *Frontiers in neuroscience*, vol. 9, no. 409, pp. 1-19, 2015.
- [2] T. Matsubara and H. Torikai, "Asynchronous cellular automaton-based neuron: theoretical analysis and on-FPGA learning," *IEEE transactions on neural networks and learning systems*, vol. 24, no. 5, pp. 736–748, 2013.
- [3] E. M. Izhikevich, *Dynamical Systems in Neuroscience: The Geometry of Excitability and Bursting (Computational Neuroscience)*. Cambridge, MA: MIT Press, Nov. 2006.
- [4] R. FitzHugh, "Impulses and physiological states in theoretical models of nerve membrane," *J. Biophys.*, vol. 1, no. 6, pp. 445-466, 1961.
- [5] J. L., Hindmarsh, and R. M. Rose, "A model of neuronal bursting using three coupled first order differential equations," *Proceedings of the Royal Society of London B: Biological Sciences*, vol. 221, no. 1222, pp. 87–102, 1984.

- [6] H. Soleimani, A. Ahmadi and M. Bavandpour, “Biologically inspired spiking neurons: Piecewise linear models and digital implementation,” *IEEE Trans. Circuits Syst. I, Reg. Papers*, vol. 59, no. 12, pp. 2991–3004, 2012.
- [7] M. Nouri, Gh. Karimi, A. Ahmadi, and D. Abbott, “Digital multiplierless implementation of the biological FitzHugh-Nagumo model,” *Neurocomputing*, Mar. 2015, 10.1016/j.neucom.2015.03.084.
- [8] Hayati, M., Nouri, M. Abbott, D., and Haghiri, S., “Digital Multiplierless Realization of Two Coupled Biological Hindmarsh-Rose Neuron Model,” *Circuits and Systems II: Brief Express, IEEE Transactions on*, vol. 63, no. 5, pp. 463–467, 2016.

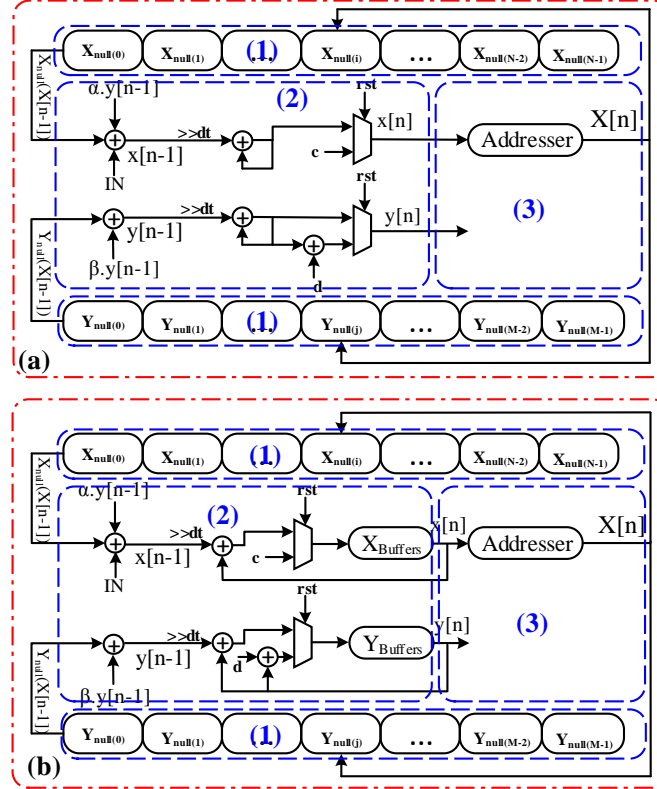


Figure 1: The detailed internal structure of (a) the synchronous cellular hardware for a single 2-D neuron unit and (b) the synchronous cellular hardware for a network of neuron units.

Table 1: Cellular Values for various neuron models.

Parameters	Izhikevich	FHN	HR
$\Delta x$	2	0.1250	0.1250
$x_{min}$	-80	-2	-2
$x_{max}$	-16	2	2
$dt$	$\frac{1}{32}$	$\frac{1}{1024}$	$\frac{1}{32}$
$N$	32	32	32

Table 2: RMSE and NRMSE Error for 1000 Points of Some Cases of Neuron Models with Various Resolutions.

Responses	32		64		128	
	RMSE	NRMSE%	RMSE	NRMSE%	RMSE	NRMSE%
IZHI <sub>TS</sub>	2.482	2.61	1.893	1.98	0.735	0.77
FHN <sub>EB</sub>	0.107	3.25	0.080	2.13	0.043	1.15
HR <sub>TS</sub>	0.094	2.87	0.052	1.65	0.031	0.82
Mean Error	0.894	2.91	0.675	1.92	0.269	0.91

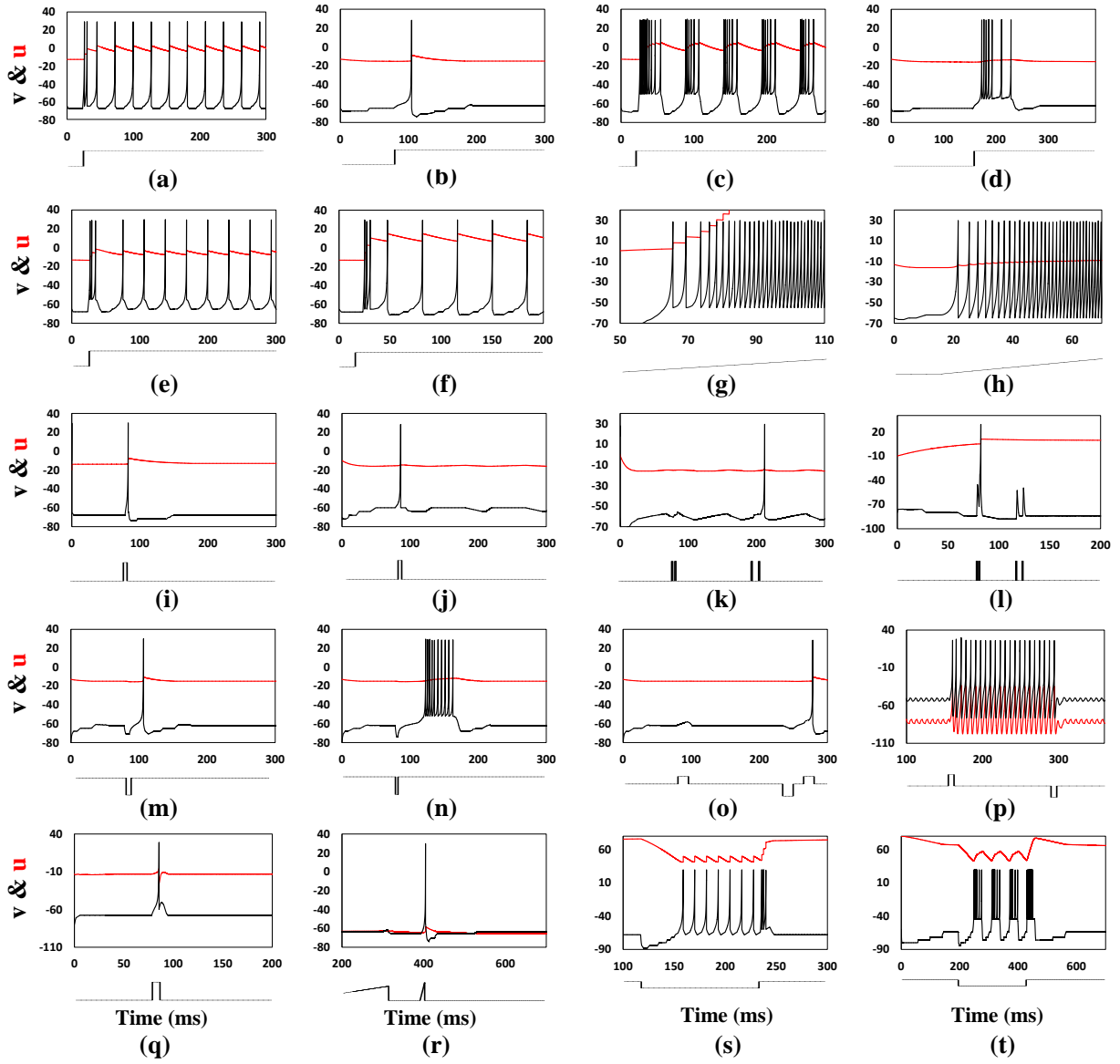


Figure 2: Time-domain representation of various dynamical responses of a cellular Izhikevich neuron circuit with 32 pixels. (a) Tonic spiking, (b) phasic spiking, (c) tonic bursting, (d) phasic bursting, (e) mixed mode, (f) spike frequency adaption, (g) class I excitable, (h) class II excitable, (i) spike latency, (j) sub-threshold oscillation, (k) resonator, (l) integrator, (m) rebound spike, (n) rebound burst, (o) threshold variability, (p) bistability, (q) Depolarized After-Potential (DAP), (r) accommodation, (s) inhibitory induced spiking, and (t) inhibitory induced bursting.

Table 3: Device Utilization of the Xilinx Virtex-II Pro FPGA for the Synchronous Cellular Izhikevich Model and Previous Published Piecewise Linear Model [6].

Parameter	Cellular IZHI	IZHI (4pwl)[6]	Performance
FF	265	491	1.85 times less
4-input LUT	274	602	2.19 times less
Freq. (MHz)	254.26	204.31	1.24 times more

Table 4: Device Utilization of the Xilinx Virtex-II Pro FPGA for the Synchronous Cellular FHN Model and Previous Published Piecewise Linear Model [7].

Parameter	Cellular FHN	FHN[7]	Performance
FF	370	526	1.42 times less
4-input LUT	373	1085	2.9 times less
Freq. (MHz)	248.14	Not reported	-

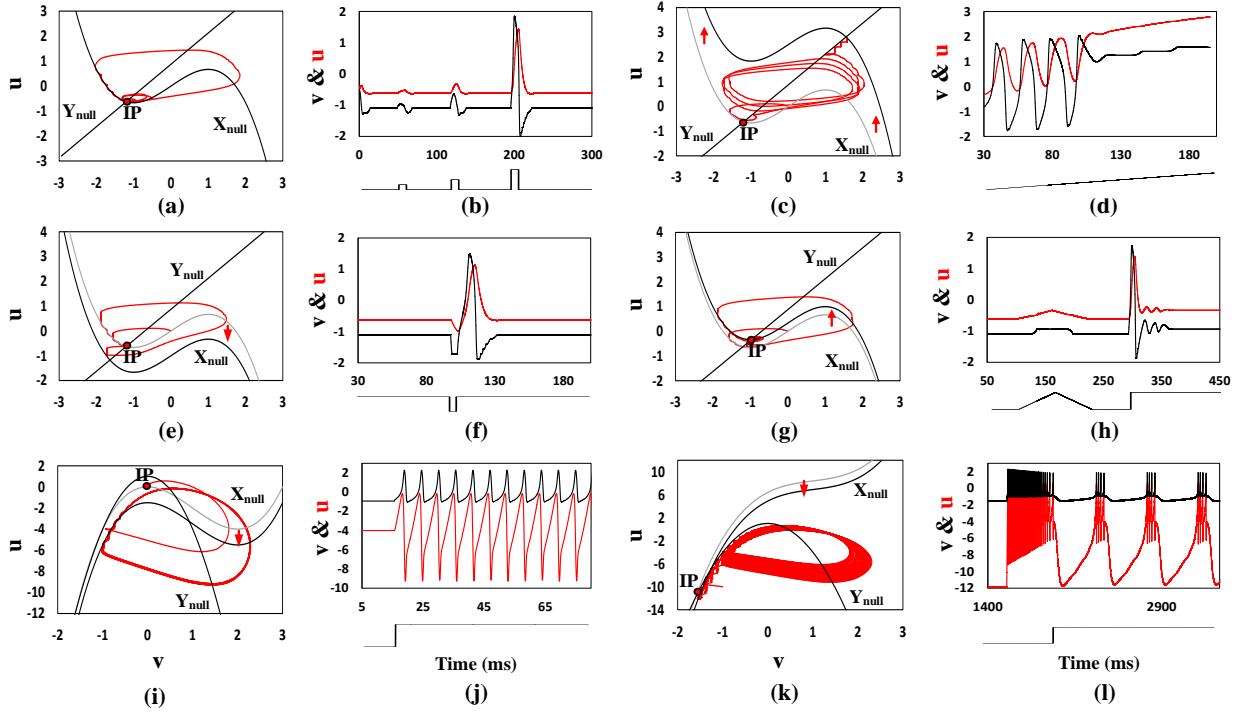


Figure 3: Phase plane (left side) and time-domain (right side) representations of (a-b) absence of all-or-none spikes phenomenon, (c-d) excitation block phenomenon, (e-f) post-inhibitory rebound spike phenomenon, and (g-h) spike accommodation phenomenon for the cellular FHN neuron and (i-j) spiking mode, (k-l) bursting mode for the cellular HR neuron with 32 pixels. In the phase plane, **IP** is the initial location of the state variable.

Table 5: Device Utilization of the Xilinx Virtex-II Pro FPGA for the Synchronous Cellular HR Model and Previous Published Piecewise Linear Model [8].

Parameter	Cellular HR	HR[8]	Performance
FF	425	431	1.01 times less
4-input LUT	435	659	1.51 times less
Freq. (MHz)	309.37	81.2	3.80 times more

Table 6: Device Utilization of the Kintex-7 (XC7K325T) FPGA for the All Synchronous Cellular Neuron Models.

Parameter	Cellular IZHI	Cellular FHN	Cellular HR
FF	187	256	364
6-input LUT	223	414	416
Freq. (MHz)	597.58	563.88	663.10